RSC Advances

PAPER

View Article Online
View Journal | View Issue

Cite this: *RSC Adv.*, 2024, **14**, 27799

Bridging the size gap between experiment and theory: large-scale DFT calculations on realistic sized Pd particles for acetylene hydrogenation†

Apostolos Kordatos, [a] Khaled Mohammed, [a] Reza Vakili, [b] Haresh Manyar, [b] Alexandre Goguet, [b] Emma Gibson, [c] Marina Carravetta, [a] Peter Wells [a] and Chris-Kriton Skylaris *[a]

Metal nanoparticles, often supported on metal oxide promoters, are a cornerstone of heterogeneous catalysis. Experimentally, size effects are well-established and are manifested through changes to catalyst selectivity, activity and durability. Density Functional Theory (DFT) calculations have provided an attractive way to study these effects and rationalise the change in nanoparticle properties. However such computational studies are typically limited to smaller nanoparticles (approximately up to 50 atoms) due to the large computational cost of DFT. How well can such simulations describe the electronic properties of the much larger nanoparticles that are often used in practice? In this study, we use the ONETEP code, which is able to achieve more favourable computational scaling for metallic nanoparticles, to bridge this size gap. We present DFT calculations on entire Pd and Pd carbide nanoparticles of more than 300 atoms (approximately 2.5 nm diameter), and find major differences in the electronic structure of such large nanoparticles, in comparison to the commonly investigated smaller clusters. These differences are also manifested in the calculated chemical properties such as adsorption energies for C_2H_2, C_2H_4 and C_2H_6 on the pristine Pd and PdC_x nanoparticles which are significantly larger (up to twice in value) for the ~300 atoms structures. Furthermore, the adsorption of C_2H_2 and C_2H_4 on PdC_x nanoparticles becomes weaker as more C is introduced in the Pd lattice whilst the impact of C concentration is also observed in the calculated reaction energies towards the hydrogenation of C_2H_2, where the formation of C_2H_6 is hindered. Our simulations show that PdC_x nanoparticles of about 5% C per atom fraction and diameter of 2.5 nm could be potential candidate catalysts of high activity in hydrogenation reactions. The paradigm presented in this study will enable DFT to be applied on similar sized metal catalyst nanoparticles as in experimental investigations, strengthening the synergy between simulation and experiment in catalysis.

Received 7th May 2024
Accepted 18th August 2024

DOI: 10.1039/d4ra03369h

rsc.li/rsc-advances

1. Introduction

The selective hydrogenation of acetylene has been extensively investigated as an important purification process of ethylene feedstocks in the production of polyethylene.[1–4] During the exposure to hydrocarbons, the catalyst will adsorb acetylene, which strongly binds with Pd surface atoms. This will reduce the adsorption of ethylene whilst promoting the full hydrogenation of acetylene to ethane. Therefore, to increase selectivity towards ethylene *via* tuning the catalytic process, it is important to understand the mechanisms of ethylene and ethane formation as well as side-reactions like surface C–C oligomerization (that leads to green oil formation and deactivation of the catalyst).[5,6]

Supported Pd nanoparticles (NPs) are promising catalysts, widely used due to their high activity in a range of industrial applications[7] such as the hydrogenation and oxidation of hydrocarbons and conversion of biomass;[8] whilst being highly selective towards the partial hydrogenation of acetylene to ethylene. Additionally, the *in situ* formation of interstitial phases[9] during catalysis, such as carbidic Pd,[10] have attracted considerable interest due to their potential contribution in the increased selectivity towards the desirable products.[11] Carbidic Pd is beneficial in blocking side-formation of phases such as hydrides,[12,13] which otherwise would provide surface H that eventually hydrogenate ethylene to ethane. Insights on the formation mechanisms of PdC NPs are required, as well as the impact of NP size and shape with respect to the catalytic activity,

[a]*School of Chemistry and Chemical Engineering, University of Southampton, UK. E-mail: c.skylaris@soton.ac.uk*

[b]*School of Chemistry and Chemical Engineering, Queen's University, Belfast, UK*

[c]*School of Chemistry, University of Glasgow, UK*

† Electronic supplementary information (ESI) available. See DOI: https://doi.org/10.1039/d4ra03369h

aiming to tune the materials properties through controlled synthesis and achieve high stability, activity and selectivity.

The acetylene semi-hydrogenation over Pd/Al_2O_3 has been investigated *via* experimental and theoretical methods in the recent study of Gonçalves *et al.*[14] where the reaction is modelled on a pyramidal Pd_{30} cluster. This study shows that full hydrogenation of C_2H_4 to C_2H_6 exhibits higher activation barriers as a first indication of Pd selectivity towards the production of ethylene. In the experimental and theoretical work of Liu *et al.*,[15] DFT calculations show that desorption of ethylene is more favourable for the carbidic phase rather than the pristine high-coordinated Pd(111) surface. Furthermore, Vignola *et al.*[16] investigated the C–C bond formation that leads to catalyst poisoning through the formation of oligomers. Oligomers block the active sites of the catalyst whilst consuming hydrogen that could hydrogenate acetylene to ethylene. In their study, they show that small Pd ensembles are considered as more appropriate catalysts to avoid oligomer formation, and that the particle size contribution should be further investigated as an important feature in catalytic activity. The role of subsurface C in alkyne hydrogenation has also attracted interest; in the experimental study of Teschner *et al.*,[17] it is shown that the subsurface Pd sites filled with C or H, have a major role in the hydrogenation reactions taking place on the surface. The subsurface chemistry impact on the selective hydrogenation of ethylene has also been reported by Studt *et al.*[18] In their theoretical study, DFT calculations have been performed showing that selectivity increases *via* weakening of the surface bond with adsorbates. In the case of Pd NPs, the size effect has been investigated by Sun *et al.*[19] where experimental and computational work showed that C_4 and green oil form on structures smaller than 2 nm, whilst within at a size of 2.6 nm, adsorption of ethylene becomes weaker. The C–C/C–H bonding has been investigated in the theoretical study of Zhao *et al.*,[20] for a range of transition metal surfaces (where the most promising identified were the Pd(111) and Pt(111)), showing that the order in terms of acetylene hydrogenation activity is inverse to that of the selectivity towards ethylene. Yang *et al.*[21] performed DFT calculations on a range of different Pd surfaces, examining the effect of subsurface C and H and showed that the close-packed Pd(111) exhibits the highest selectivity. The selective hydrogenation of acetylene in the presence of ethylene has been also investigated by Abdollahi *et al.*[22] In their study, activation energies for the reaction process are reported for a range of Pdn ($n = 2$–15) nanoclusters. The Pd_2 is reported to exhibit the best selectivity towards ethylene. Besides the synthesis method and characteristics such as the shape and size of the NPs, the support is also important towards activity and selectivity as reported in the experimental work by Benavidez *et al.*[23] They showed that C supported Pd catalysts exhibit higher selectivity towards ethylene compared to oxide supported Pd catalysts. Additionally, supports such as gamma alumina may lead to green oil formation as reported by Asplund *et al.*[24] The aforementioned works provided useful insights on the hydrogenation of acetylene on Pd catalysts as slabs and NPs, however the role of the PdC_x formation on the hydrogenation reaction in realistic systems, comparable with experimental results is still required.

In this study, we address for the first time the challenge of the simulation system size in Pd based catalysis *via* performing large-scale DFT calculations on entire large Pd/PdC_x NPs at different C concentrations. The structures used for our investigation were of more than 300 atoms and up to approximately 2.5 nm, going beyond the investigated system sizes reported so far in the literature by one order of magnitude. All geometries were fully relaxed, providing useful insights on the PdC_x formation and the effect of C concentration on the hydrogenation of C_2H_2. The binding modes of adsorbed C_2H_2, C_2H_4 and C_2H_6 on the [100]/[111] facets of pristine and carbidised structures were firstly investigated and adsorption energies for the most stable configurations were obtained. Finally, we examined the impact of interstitial C at increasing (5% and 13% per atom fraction) concentrations on the reactants, intermediates, and products of the hydrogenation of C_2H_2 to C_2H_4 and C_2H_6.

2. Methodology

The linear-scaling DFT code ONETEP[25] was used for the modelling of the pristine Pd and PdC_x structures. For the construction of the density matrix, localized non-orthogonal Wannier functions (NGWFs) as expressed through a set of periodic sinc (p-sinc) functions[26] were used. For these calculations, the p-sinc basis set was set to a kinetic energy cut-off of 800 eV. For the exchange and correlation interactions, the density functional of Perdew, Burke and Ernzerhof (PBE)[27] was used together with the Grimme D2 [28] empirical correction for dispersion interactions. The core electrons were represented *via* norm-conserving pseudopotentials. The NGWFs and density matrix are concurrently optimized self-consistently *via* the Ensemble DFT (EDFT) method[29] for metallic systems with a Fermi–Dirac smearing of 0.1 eV. The geometries were allowed to relax in the minimum energy configuration. For all atoms, an NGWF radius of 9.0 Bohr has been used, whilst geometry relaxations were performed at the Γ-point in cubic cells of 22–37 Å. The construction of Pd NPs was done using the ASE[30] tool with the average Pd–Pd bond length of 2.74 Å. The schematic representation of the Pd and PdC_x cells is generated using the CrystalMaker[31] software, whilst for the reaction energies between different crystallographic configurations, the following formula is used:

$$E_{\text{Reaction}} = E_{\text{Products}} - E_{\text{Reactants}}$$

where E_{Products} corresponds to the energy of the relaxed structures of products and $E_{\text{Reactants}}$ to the energy of the relaxed structures of the reactants. For the adsorption energies of C_2H_2, C_2H_4, C_2H_6 and intermediates on the Pd surface the following formula is used:

$$E_{\text{Adsorption}} = E_{\text{Pd–adsorbate}} - (E_{\text{Pd/PdC}} + E_{\text{adsorbate}})$$

where $E_{\text{Pd–adsorbate}}$ corresponds to the energy of the relaxed structure of Pd NP with the adsorbate, $E_{\text{Pd/PdC}}$ to the energy of

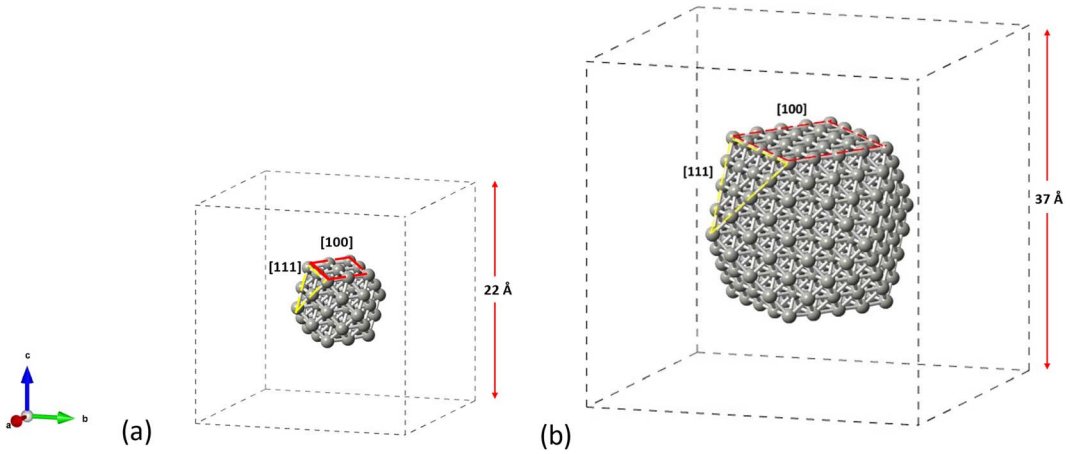

Fig. 1 Crystallographic arrangements of the NP structures showing the cuboctahedral (a) Pd_{55} and (b) Pd_{309}, as placed in the centre of their simulation boxes.

the relaxed structures for the Pd/PdC_x NPs and $E_{adsorbate}$ to the energy to the isolated molecule.

3. Results and discussion

3.1 Crystallography

The structures considered as appropriate for this study are the cuboctahedral Pd_{55} and Pd_{309} NPs as shown in Fig. 1. We aim to account for both the [100] and [111] facets on the same particle in order to get insights on the materials performance under reaction conditions. The NP structures have been modelled in conditions of vacuum to avoid interactions with their periodic images, whilst allowing at least 5 Å of vacuum in each direction around the particle which was placed in the center of the simulation box. All structures were allowed to relax until optimized geometries were obtained. For the molecules of C_2H_2, C_2H_4 and C_2H_6, we performed separate geometry relaxations for the isolated structures prior to their introduction on the NP's surface.

3.2 Pd carbide NPs

Carbidic Pd models were created through C incorporation corresponding to the occupation of the octahedral interstitial sites. In our previous work, we investigated the incorporation of C for different structures of Pd NPs,[32] where we showed that there is a shape-dependent limitation of interstitial C concentration through the octahedral Pd sites; therefore, the carbidic phases considered in this work are up to a C concentration of 13% since we found that this is the maximum concentration that can be accommodated by all shapes. For the cuboctahedral structure, we have shown[32] that the activation energy of carbidisation corresponds to 21.2 kJ mol^{-1} for the [111] facet and that, at increasing concentrations, the criterion is to allow at least one vacant site between C atoms that will preferentially occupy the subsurface area of the NP being long distance for low concentrations whilst aiming not to be in close neighboring sites at increasing amounts. In this study, two C concentrations (5% and 13%) have been considered. In Fig. 2 we show the carbidic structures for Pd_{55} and

Table 1 The average Pd–Pd bond length *vs.* C concentration in cuboctahedral Pd_{55} and Pd_{309}

C (%)	Pd_{55} Pd–Pd (Å)	Pd_{309} Pd–Pd (Å)
0.0	2.73	2.75
5.0	2.74	2.77
13.0	2.75	2.80

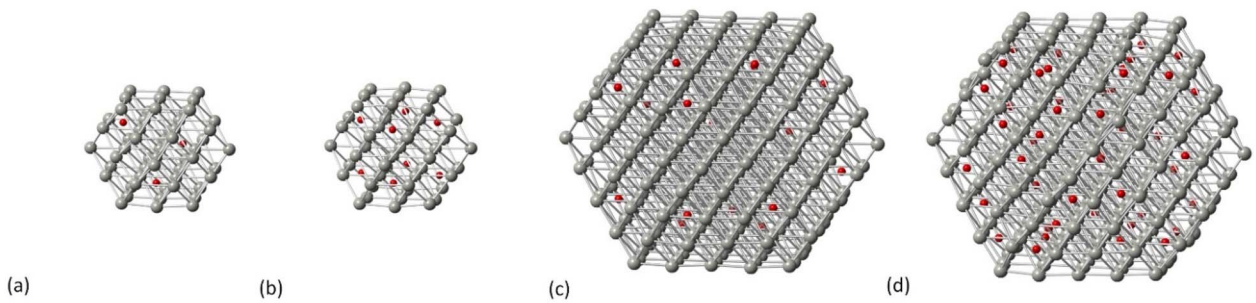

Fig. 2 The carbidic phases of Pd NPs at (a) Pd_{55} at 5% C concentration, (b) Pd_{55} at 13% C concentration, (c) Pd_{309} at 5% C concentration and (d) Pd_{309} at 13% C concentration. Grey spheres represent Pd atoms and red spheres represent C atoms.

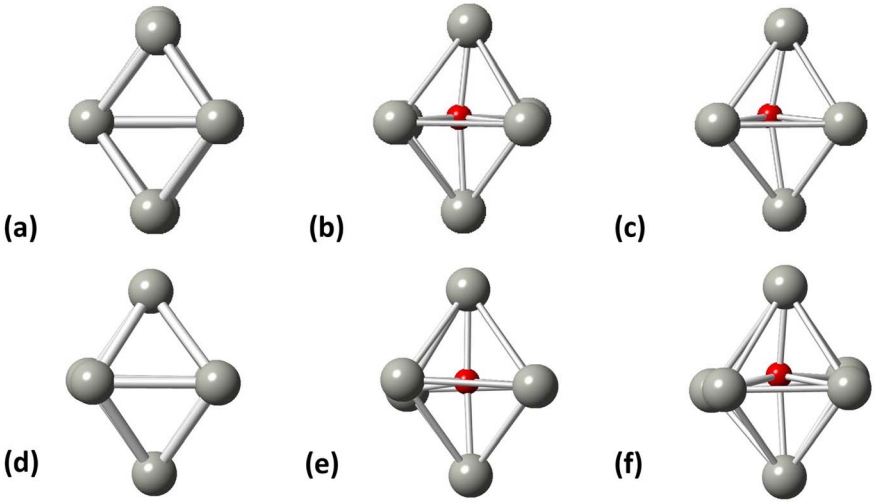

Fig. 3 Pd octahedral interstitial sites for (a) Pd_{55} at 0% C concentration, (b) Pd_{55} at 5% C concentration, (c) Pd_{55} at 13% C concentration, (d) Pd_{309} at 0% at C concentration, (e) Pd_{309} at 5% at C concentration, and (f) Pd_{309} at 13% at C concentration. Grey spheres represent Pd atoms and red spheres represent C atoms.

Pd_{309} whilst the average Pd–Pd bond distance for all structures is summarized in Table 1.

3.3 C_2H_2, C_2H_4 and C_2H_6 adsorption on Pd NPs

Initially, we studied the preferred adsorption and orientation of the molecules on the NP surface by doing full geometry relaxations of each NP-adsorbate complex. These geometries were used subsequently as configurations of reactants and products in the partial and full hydrogenation states of C_2H_2 to C_2H_4 and C_2H_6. The relaxation of C in the octahedral interstitial Pd sites at 0%, 5% and 13% concentration is shown in Fig. 3. The average Pd–C bond length for Fig. 3(b) and (c) is 2.04 Å and 2.07 Å respectively whilst for 3(e) and (f) is 2.01 Å and 2.06 Å respectively. Fig. 4 shows the relaxed structures of C_2H_2, C_2H_4 and C_2H_6 on the [100] and [111] facets of the pristine Pd_{309} surface. The Pd_{55} relaxed structures and NP–adsorbate bond lengths for all geometries used for this study are included in the ESI, Fig. S1–S6.† Additionally, the surface modifications for the [100] and [111] facets of the Pd_{309} are also shown in Fig. 5, whilst the geometries of C_2H_2, C_2H_4 and C_2H_6 on the [100] facet of pristine and carbidic Pd_{309} are shown in Fig. 6. It is evident that interstitial C will change the facet morphology leading to different binding arrangements between surface Pd and hydrocarbons. We compared the adsorption energies of the C_2H_2 to C_2H_4 and C_2H_6 molecules at different C concentrations, NP size and facet. The adsorption energies for both [100] and [111] facets of the cuboctahedral structures are shown in Fig. 7, whilst the obtained values are presented in Tables S1 and S2 in the ESI.† Our calculations showed that C_2H_2 adsorbs more

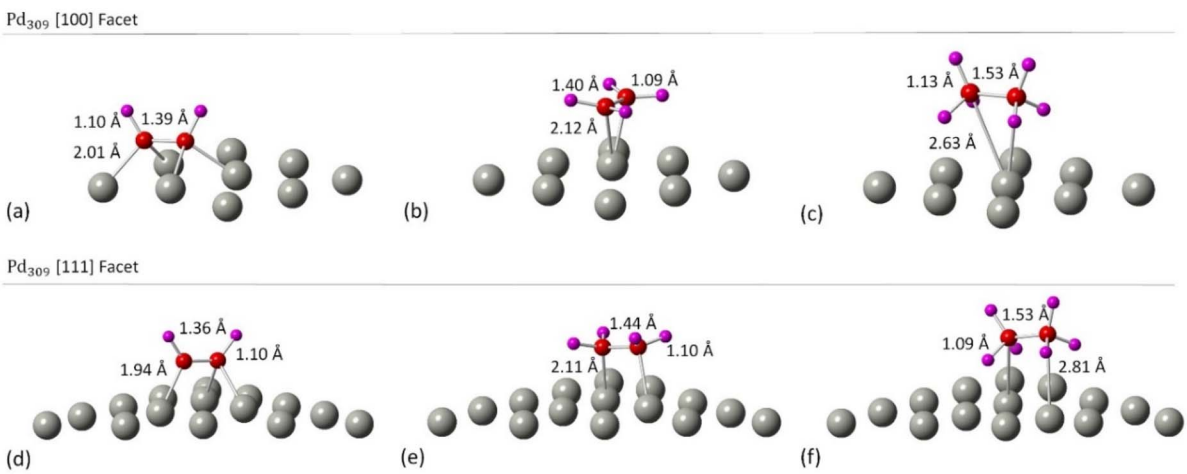

Fig. 4 The relaxed structures of (a) C_2H_2 on the [100] facet of Pd_{309} NP, (b) C_2H_4 on the [100] facet of Pd_{309} NP, (c) C_2H_6 on the [100] facet of Pd_{309} NP, (d) C_2H_2 on the [111] facet of Pd_{309} NP, (e) C_2H_4 on the [111] facet of Pd_{309} NP and (f) C_2H_6 on the [111] facet of Pd_{309} NP. Grey spheres represent Pd atoms, red spheres represent C atoms and purple spheres represent H atoms. Geometry relaxations were performed on the entire Pd NP–ligand complexes.

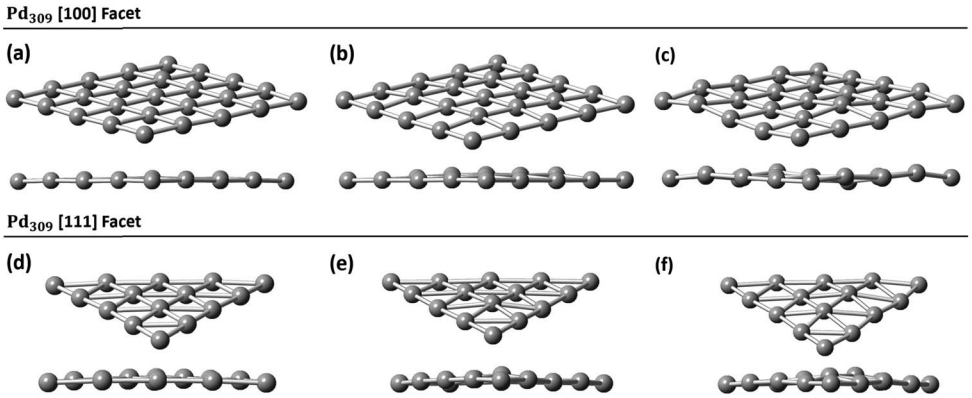

Fig. 5 Pd_{309} surface modifications for (a) the [100] facet at 0% C, (b) the [100] facet 5% C, (c) the [100] facet 13% C, (d) the [111] facet at 0% C, (e) the [111] facet at 5% C, and (f) the [111] facet at 13% C.

strongly on the 4-fold site of the [100] facet and in agreement with the work of Crespo-Quesada *et al.*[33] We also find that C_2H_2 is adsorbed more strongly (-300 kJ mol^{-1} for the [100] of Pd_{55} and -631.1 kJ mol^{-1} for the [100] of Pd_{309}) on the surface of the NP than C_2H_4 (-172.9 kJ mol^{-1} for the [100] of Pd_{55} and -396.9 kJ mol^{-1} for the [100] of Pd_{309}) and C_2H_6 (-72.0 kJ mol^{-1} for the [100] of Pd_{55} and -291.6 kJ mol^{-1} for the [100] of Pd_{309}). We observed that the adsorption energies are considerably

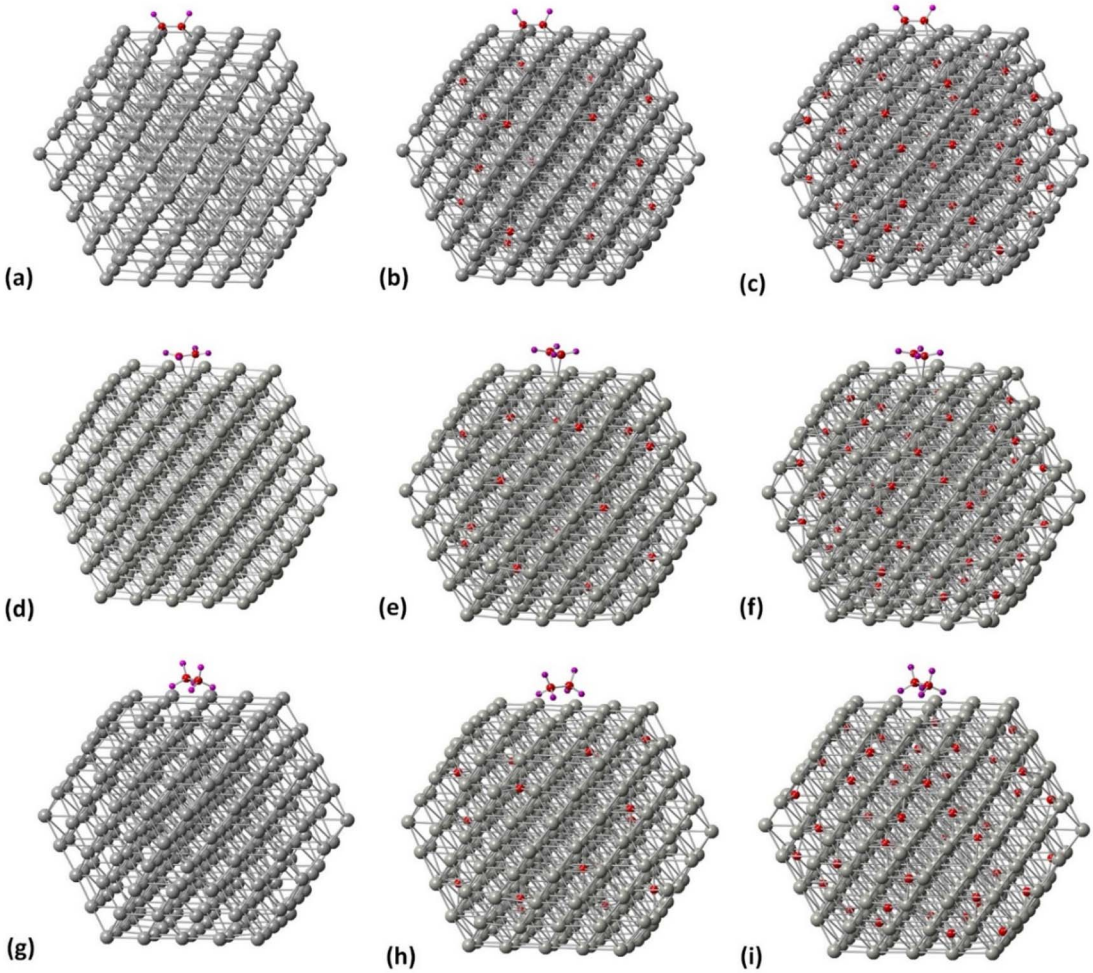

Fig. 6 Related geometries of molecule/PdC_x NP complexes. (a)–(c) C_2H_2 on the [100] facet of Pd_{309} at 0, 5 and 13% C concentration, (d)–(f) C_2H_4 on the [100] facet of Pd_{309} at 0, 5 and 13% C concentration, and (g)–(i) C_2H_6 on the [100] facet of Pd_{309} at 0, 5 and 13% C concentration.

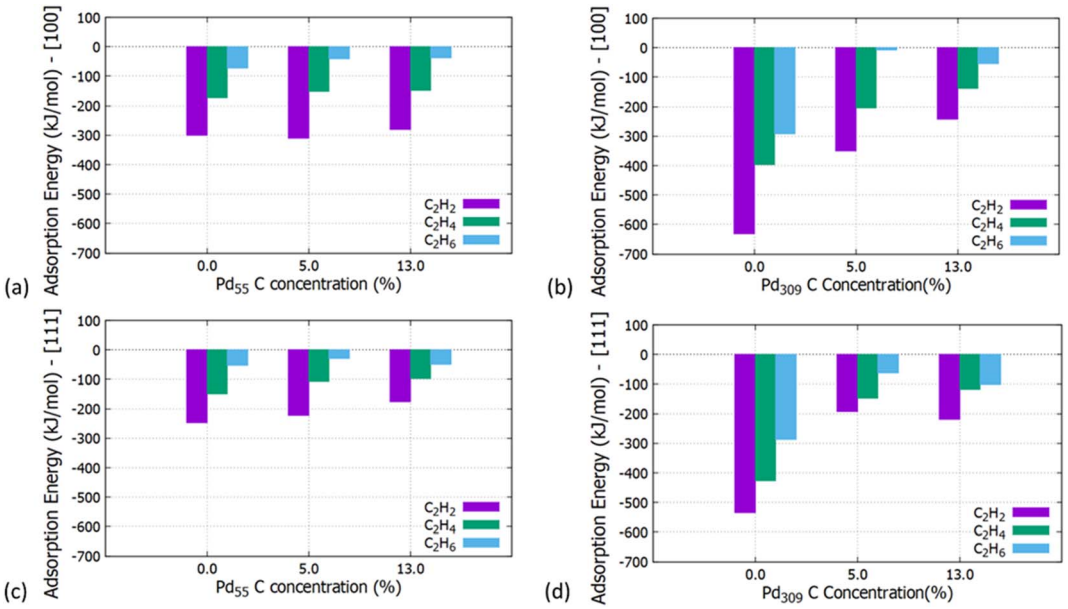

Fig. 7 Adsorption energies of C_2H_2, C_2H_4 and C_2H_6 on the (a) [100] facet of Pd_{55} at C concentration = 0%, 5% and 13%, (b) [100] facet of Pd_{309} at C concentration = 0%, 5% and 13%, (c) [111] facet of Pd_{55} at C concentration = 0%, 5% and 13% and (d) [111] facet of Pd_{309} at C concentration = 0%, 5% and 13%.

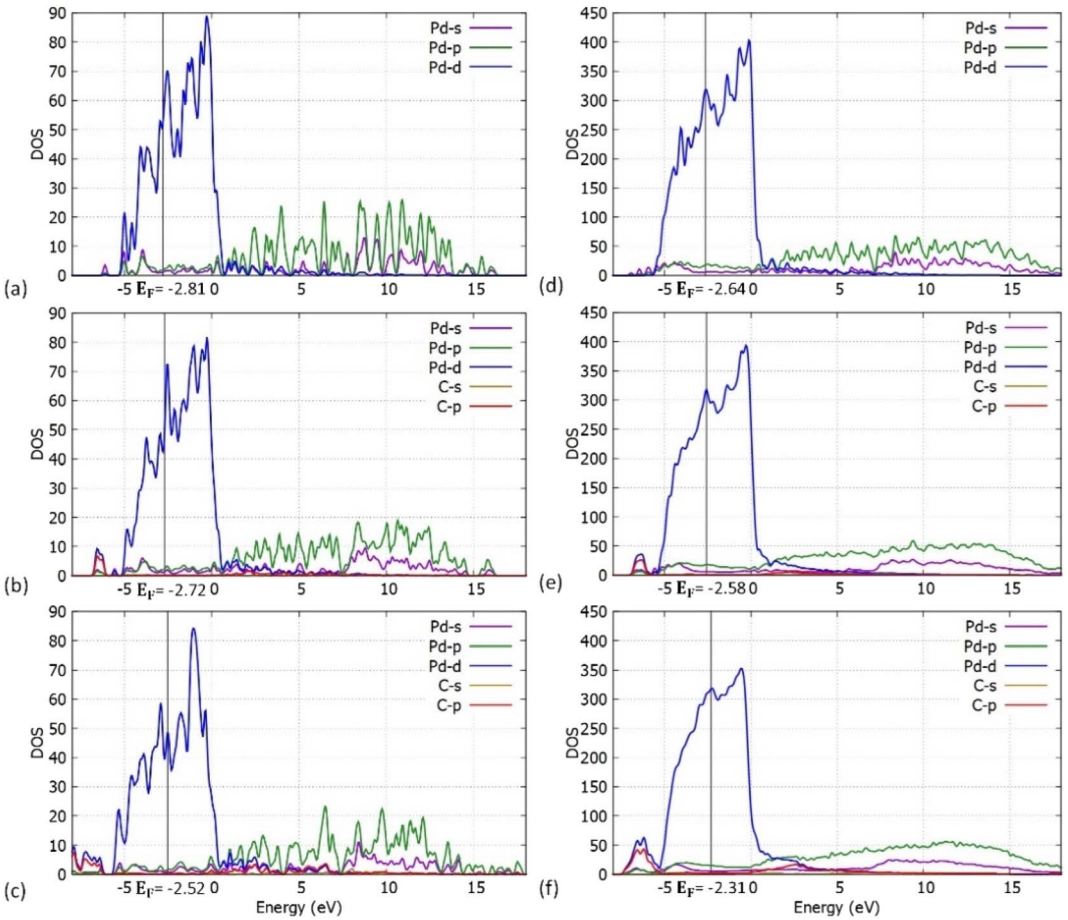

Fig. 8 Atom and orbital resolved DOS plots for the (a) Pd_{55} at C = 0% concentration, (b) Pd_{55} at C = 5% concentration, (c) Pd_{55} at C = 13% concentration, (d) Pd_{309} at C = 0% concentration, (e) Pd_{309} at C = 5% concentration and (f) Pd_{309} at C = 13% concentration.

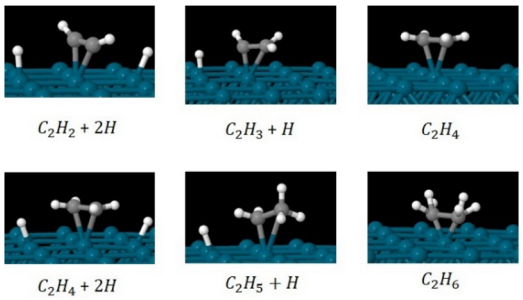

Fig. 9 Relaxed geometries of reactants, intermediates and products for the hydrogenation of C_2H_2 to C_2H_4 (part B) and C_2H_6 (part D) on the [100] facet of pristine Pd_{309}. Geometry relaxations were performed on the entire Pd_{309}–ligand complex. Blue spheres are Pd, grey spheres are C and white spheres are H.

higher for the Pd_{309} structure, showing that the particle size is expected to affect the reaction. As we introduce interstitial C in the Pd lattice, the adsorption energies are reduced drastically for Pd_{309} but very little for Pd_{55}. We also observed that the carbidic Pd has significantly lower adsorption energies for C_2H_4 on the [100] and [111] facets as compared to the pristine structure. This shows that ethylene will desorb more easily from the surface of the PdC_x NP, hence it is a first indication of possible suppression of the full hydrogenation to ethane.

We have also performed density of states (DOS) investigations on the pristine and carbidic Pd_{55} and Pd_{309}. As shown in Fig. 8, the metallic behaviour for both pristine structures is confirmed. Furthermore, Pd_{309} corresponds considerably more to bulk-like DOS when compared to Pd_{55}. This behaviour is expected since the volume of the particle is larger, and its electronic structure is closer to bulk Pd.

To further explore the effect of C concentration on the hydrogenation of C_2H_2, we investigated the reaction energies of each stage of the formation of C_2H_4 and C_2H_6.

3.4 Hydrogenation reactions

We investigated the partial and full hydrogenation of C_2H_2 on the pristine Pd_{55} and Pd_{309}. Fig. 9 shows the reactants, products and intermediates on the Pd_{309} surface. The hydrogenation of acetylene on Pd NPs was investigated as a four-part process leading to partial and full hydrogenation corresponding to C_2H_4 and C_2H_6 as the two final products:

$$\text{(Part A) } C_2H_2 + 2H \rightarrow C_2H_3{+}H$$

$$\text{(Part B) } C_2H_3 + H \rightarrow C_2H_4$$

$$\text{(Part C) } C_2H_4 + 2H \rightarrow C_2H_5{+}H$$

$$\text{(Part D) } C_2H_5 + H \rightarrow C_2H_6$$

The reaction energies for the partial and full hydrogenation of C_2H_2 to C_2H_4 and C_2H_6 on the [100] and [111] facets of Pd_{55} and Pd_{309} at 0, 5 and 13% of interstitial C concentration are shown in Fig. 10. Our results show that information about the catalytic behaviour of PdC_x NPs used in practical studies can be obtained by simulating entire large PdC_x NPs, as done in this work.

For Pd_{55}, reaction energies for the [100] facet are exothermic for parts A ($E_{Reaction} = -57.6$ kJ mol^{-1}) and B ($E_{Reaction}$ =

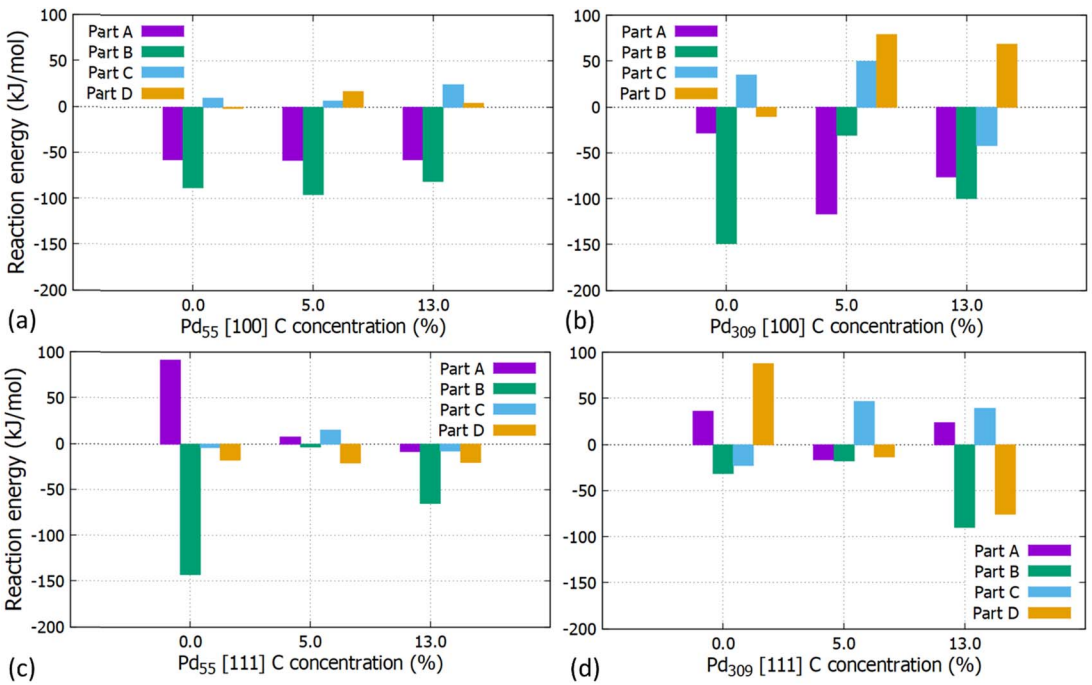

Fig. 10 Reaction energies for the partial and full acetylene hydrogenation on the (a) [100] facet of the Pd_{55} at C (=0%, 5% and 13%), (b) [100] facet of the Pd_{309} at C (=0%, 5% and 13%), (c) [111] facet of the Pd_{55} at C (=0%, 5% and 13%) and (d) [111] facet of Pd_{309} at C (=0%, 5% and 13%).

−88.1 kJ mol^{-1}) whilst the introduction of interstitial C has a minor contribution. For the [111] facet, part A corresponds to endothermic reaction energies for pristine Pd and PdC_x (5%). Here, interstitial C results to lower values and the behaviour is affected by the particle's distortion at the higher C concentration of 13%.

For the pristine Pd_{309} the partial hydrogenation on the [100] facet, part B is more exothermic ($E_{Reaction}$ = −149.3 kJ mol^{-1}) than part A ($E_{Reaction}$ = −28.6 kJ mol^{-1}) for the semi-hydrogenation to C_2H_4. As we introduce interstitial C in the Pd lattice, C_2H_3 forms more easily as the reaction energy becomes more exothermic, whilst when we reach the maximum considered C concentration of 13%, reaction energies correspond to similar values. For the [111] facet, part A is also endothermic. In contrast with Pd_{55}, the reaction energy turns to endothermic for 5% C concentration showing that interstitial C, larger available surface area and reduced distortion of Pd_{309} will promote the reaction. Overall, we observe that parts A and B correspond to exothermic reactions showing that the formation of intermediate C_2H_3 and C_2H_4 as the final product on the [100] facet of Pd_{309} is energetically favourable. Furthermore, the carbidic phase has a considerable impact on the reaction energies. This is due to the stronger adsorption of intermediates such as C_2H_3 interacting with more surface Pd atoms compared to the pristine Pd_{309}. This is due to the [100] facet getting distorted as a consequence of C doping. For the full hydrogenation to C_2H_6 (parts C and D), our calculations showed that the reaction to C_2H_5 is slightly endothermic ($E_{Reaction}$ = 34.82 kJ mol^{-1}) and full hydrogenation to ethane corresponds to a slightly exothermic energy of reaction ($E_{Reaction}$ = −10.46 kJ mol^{-1}). This behaviour is in agreement with previously reported computational work[14] where the reaction energy for the formation of C_2H_5 is endothermic (approximately 25 kJ mol^{-1}) and the reaction energy for the formation of C_2H_6 is exothermic (approximately −9.6 kJ mol^{-1}). The same behaviour is observed for the increasing concentration of 5% C although here the full hydrogenation to ethane also turns to endothermic.

Our calculations unambiguously show that interstitial C at a concentration of around 5% promotes the formation of ethylene, since parts C and D that would lead to ethane are endothermic. Furthermore, at this concentration, the adsorption energy of C_2H_4 is reduced by more than 30% compared to the pristine Pd, whilst when increasing the interstitial C concentration close to saturation (at about 13%), part C becomes exothermic again. Therefore, more work is needed towards understanding the effect of the carbidic phase to increase selectivity in Pd catalysts.

4. Conclusions

We performed large-scale DFT calculations on entire cuboctahedral Pd_{55} and Pd_{309} NPs with different degrees of carbidisation to gain insights on the hydrogenation of C_2H_2 to C_2H_4 and C_2H_6. We investigated two phases of PdC_x at concentrations of 5% and 13% (which is close to the maximum experimentally and computationally determined value) to examine how the particle size affects the adsorption and reaction energies during catalytic hydrogenation given that metal nanoparticle catalysts, often supported on metal oxide promoters, are essential to many applications in heterogeneous catalysis. Experimentally, size effects are well-established and are manifested through changes to catalyst selectivity, activity and durability and DFT calculations have provided an attractive way to study these effects and rationalise the change in nanoparticle properties. However, most DFT studies are typically limited to smaller nanoparticles (approximately up to 50 atoms) due to the large computational cost of DFT. Here we have used the ONETEP code, which is able to achieve more favourable computational scaling for metallic nanoparticles, to bridge this size gap and simulate nanoparticles of more than 300 atoms (approximately 2.5 nm diameter). In this study, we have used cuboctahedral Pd nanoparticles with 55 and 309 atoms and also their carbidised structures. We found that the adsorption energies of C_2H_2, C_2H_4 and C_2H_6 on the pristine Pd and PdC_x NPs are considerably larger for the Pd_{309} structure. Furthermore, the carbidic phase for the Pd_{55} has minor impact on the adsorption energies whilst for the Pd_{309}, a considerable decrease is observed as more C is introduced in the Pd interstitial sites. C_2H_2 adsorbs more strongly on the [100] facet, forming four C–Pd bonds, rather than on the [111]. However, the adsorption of C_2H_2 and C_2H_4 becomes weaker (on $Pd_{309}C_x$) as more interstitial C is introduced with the latter being responsible for promoting desorption of ethylene and blocking full hydrogenation to ethane. Since the adsorption energies decrease for Pd_{309} with increasing C concentration, while Pd_{55} is insensitive to interstitial C, it is clear that catalytic selectivity towards partial hydrogenation can only be achieved with larger Pd NPs.

Overall, we see that the partial hydrogenation of C_2H_2 to C_2H_4 is favourable for both Pd_{55} and Pd_{309} with the exception of the [111] facet of Pd_{55} where monoatomic hydrogen relaxes towards the edges between facets making the hydrogenation reaction unfavourable. We showed that the size of the particle is expected to have a major impact on the reaction due to the available surface area where molecules adsorb as evidenced through the reaction energies. For the full hydrogenation of C_2H_2 we observed that the carbide phase has also an impact on the reaction towards the formation of C_2H_5 and C_2H_6, but only for Pd_{309}, not Pd_{55}. For a C concentration of 5%, the reaction is endothermic for both C_2H_5 and C_2H_6 for both facets preventing hydrogenation towards ethane. For a higher C concentration (13%) in Pd_{309}, we found that hydrogenation to C_2H_5 becomes exothermic. This is an undesirable intermediate that could also lead to full hydrogenation to ethane. Therefore, the effect of the C concentration is complex, and more work is needed to tune it towards optimum selectivity and yield, but the present study provides starting points towards further optimization of the PdC_x large nanoparticle catalyst.

This is the first time that simulations on entire large (>300 atoms) metallic NPs catalysts have been performed through DFT towards understanding catalytic hydrogenation reactions. We show that there is a dramatic difference in the behaviour of large Pd NPs as compared to small Pd NPs on the adsorption energies of hydrocarbons and the reaction energies between intermediates and products. Such DFT atomistic simulations of large realistic NPs are expected to act synergistically with

experimental studies to provide detailed and valuable insights in Pd-based directed catalysis.

Data availability

The data supporting this article have been included as part of the ESI.†

Conflicts of interest

There are no conflicts to declare.

Acknowledgements

AK, KM and RV are grateful to EPSRC (grant number EP/V000691/1) for postdoctoral funding. We are grateful to The Materials and Molecular Modelling MMM Hub (EPSRC grant number EP/T022213/1) for access to the Young supercomputer, the UKCP consortium (EPSRC grant number EP/X035956/1) for access to the ARCHER2 supercomputer and the University of Southampton for access to the Iridis5 supercomputer.

References

1 A. Borodziński and G. C. Bond, Selective Hydrogenation of Ethyne in Ethene-Rich Streams on Palladium Catalysts. Part 1. Effect of Changes to the Catalyst during Reaction, *Catal. Rev.*, 2006, **48**(2), 91–144, DOI: **10.1080/01614940500364909**.

2 M. Armbrüster, M. Behrens, F. Cinquini, K. Föttinger, Y. Grin, A. Haghofer, B. Klötzer, A. Knop-Gericke, H. Lorenz, A. Ota, S. Penner, J. Prinz, C. Rameshan, Z. Révay, D. Rosenthal, G. Rupprechter, P. Sautet, R. Schlögl, L. Shao, L. Szentmiklósi, D. Teschner, D. Torres, R. Wagner, R. Widmer and G. Wowsnick, How to Control the Selectivity of Palladium-based Catalysts in Hydrogenation Reactions: The Role of Subsurface Chemistry, *ChemCatChem*, 2012, **4**, 1048–1063, DOI: **10.1002/cctc.201200100**.

3 W. J. Kim and S. H. Moon, Modified Pd Catalysts for the Selective Hydrogenation of Acetylene, *Catal. Today*, 2012, **185**, 2–16, DOI: **10.1016/j.cattod.2011.09.037**.

4 W. Huang, J. R. McCormick, R. F. Lobo and J. G. Chen, Selective hydrogenation of acetylene in the presence of ethylene on zeolite-supported bimetallic catalysts, *J. Catal.*, 2007, **246**(1), 40–45, DOI: **10.1016/j.jcat.2006.11.013**.

5 A. N. R. Bos and K. R. Westerterp, Mechanism and kinetics of the selective hydrogenation of ethyne and ethene, *Chem. Eng. Process.*, 1993, **32**(1), 1–7, DOI: **10.1016/0255-2701(93)87001-B**.

6 I. Y. Ahn, J. H. Lee, S. S. Kum and S. H. Moon, Formation of C_4 species in the deactivation of a Pd/SiO_2 catalyst during the selective hydrogenation of acetylene, *Catal. Today*, 2007, **123**(1–4), 151–157, DOI: **10.1016/j.cattod.2007.02.011**.

7 H. A. Aleksandrov, L. V. Moskaleva, Z.-J. Zhao, D. Basaran, Z.-X. Chen, D. Mei and N. Rösch, Ethylene conversion to ethylidyne on Pd(111) and Pt(111): a first-principles-based kinetic Monte Carlo study, *J. Catal.*, 2012, **285**(1), 187–195, DOI: **10.1016/j.jcat.2011.09.035**.

8 S. M. Rogers, C. R. A. Catlow, C. E. Chan-Thaw, A. Chutia, N. Jian, R. E. Palmer, M. Perdjon, A. Thetford, N. Dimitratos, A. Villa and P. P. Wells, Tandem Site- and Size-Controlled Pd Nanoparticles for the Directed Hydrogenation of Furfural, *ACS Catal.*, 2017, **7**(4), 2266–2274, DOI: **10.1021/acscatal.6b03190**.

9 M. Maciejewski and A. Baker, Incorporation and reactivity of carbon in palladium, *Pure Appl. Chem.*, 1995, **67**(11), 1879–1884, DOI: **10.1351/pac199567111879**.

10 N. Seriani, F. Mittendorfer and G. Kresse, Carbon in palladium catalysts: a metastable carbide, *J. Chem. Phys.*, 2010, **132**, 024711, DOI: **10.1063/1.3290813**.

11 D. Torres, F. Cinquini and P. Sautet, Pressure and Temperature Effects on the Formation of a Pd/C Surface Carbide: Insights into the Role of Pd/C as a Selective Catalytic State for the Partial Hydrogenation of Acetylene, *J. Phys. Chem. C*, 2013, **117**(21), 11059–11065.

12 N. K. Nag, A Study on the Formation of Palladium Hydride in a Carbon-Supported Palladium Catalyst, *J. Phys. Chem. B*, 2001, **105**(25), 5945–5949, DOI: **10.1021/jp004535q**.

13 Y. Zhou, W. Baaziz, O. Ersen, P. A. Kots, E. I. Vovk, X. Zhou, Y. Yang and V. V. Ordomsky, Decomposition of Supported Pd Hydride Nanoparticles for the Synthesis of Highly Dispersed Metallic Catalyst, *Chem. Mater.*, 2018, **30**(22), 8116–8120, DOI: **10.1021/acs.chemmater.8b02192**.

14 L. P. L. Gonçalves, J. Wang, S. Vinati, E. Barborini, X.-K. Wei, M. Heggen, M. Franco, J. P. S. Sousa, D. Y. Petrovykh, O. S. G. P. Soares, K. Kovnir, J. Akola and Y. V. Kolen'ko, Combined experimental and theoretical study of acetylene semi-hydrogenation over Pd/Al_2O_3, *Int. J. Hydrogen Energy*, 2020, **45**(2), 1283–1296, DOI: **10.1016/j.ijhydene.2019.04.086**.

15 Y. Liu, F. Fu, A. McCue, W. Jones, D. Rao, J. Feng, Y. He and D. Li, Adsorbate-Induced Structural Evolution of Pd Catalyst for Selective Hydrogenation of Acetylene, *ACS Catal.*, 2020, **10**(24), 15048–15059, DOI: **10.1021/acscatal.0c03897**.

16 E. Vignola, S. N. Steinmann, A. A. Farra, B. D. Vandegehuchte, D. Curulla and P. Sautet, Evaluating the Risk of C–C Bond Formation during Selective Hydrogenation of Acetylene on Palladium, *ACS Catal.*, 2018, **8**(3), 1662–1671, DOI: **10.1021/acscatal.7b03752**.

17 D. Teschner, J. Borsodi, A. Wootsch, Z. Révay, M. Hävecker, A. Knop-Gericke, S. D. Jackson and R. Schlögl, The Roles of Subsurface Carbon and Hydrogen in Palladium-Catalyzed Alkyne Hydrogenation, *Science*, 2008, **320**(5872), 86–89, DOI: **10.1126/science.1155200**.

18 F. Studt, F. Abild-Pedersen, T. Bligaard, R. Sørensen, C. Christensen and J. Nørskov, On the Role of Surface Modifications of Palladium Catalysts in the Selective Hydrogenation of Acetylene, *Angew. Chem., Int. Ed.*, 2008, **47**(48), 9299–9302.

19 M. Sun, F. Wang, G. Lv and X. Zhang, Size effect of PdC nanoparticles synthesized by S-containing silane coupling agents on semi-hydrogenation of acetylene, *Appl. Surf. Sci.*, 2022, 153021, DOI: **10.1016/j.apsusc.2022.153021**.

20 Z.-J. Zhao, J. Zhao, X. Chang, S. Zha, L. Zeng and J. Gong, Competition of C-C bond formation and C-H bond formation for acetylene hydrogenation on transition

metals: a density functional theory study, *AIChE J.*, 2019, **65**(3), 1059–1066, DOI: 10.1002/aic.16492.

21 B. Yang, R. Burch, C. Hardacre, G. Headdock and P. Hu, Influence of surface structures, subsurface carbon and hydrogen, and surface alloying on the activity and selectivity of acetylene hydrogenation on Pd surfaces: a density functional theory study, *J. Catal.*, 2013, **305**, 264–276, DOI: 10.1016/j.jcat.2013.05.027.

22 T. Abdollahi and D. Farmanzadeh, Selective hydrogenation of acetylene in the presence of ethylene on palladium nanocluster surfaces: a DFT study, *Appl. Surf. Sci.*, 2018, **433**, 513–529, DOI: 10.1016/j.apsusc.2017.10.085.

23 A. D. Benavidez, P. D. Burton, J. L. Nogales, A. R. Jenkins, S. A. Ivanov, J. T. Miller, A. M. Karim and A. K. Datye, Improved selectivity of carbon-supported palladium catalysts for the hydrogenation of acetylene in excess ethylene, *Appl. Catal.*, 2014, **482**, 108–115, DOI: 10.1016/j.apcata.2014.05.027.

24 S. Asplund, Coke Formation and Its Effect on Internal Mass Transfer and Selectivity in Pd-Catalysed Acetylene Hydrogenation, *J. Catal.*, 1996, **158**(1), 267–278, DOI: 10.1006/jcat.1996.0026.

25 J. C. A. Prentice, J. Aarons, J. C. Womack, A. E. A. Allen, L. Andrinopoulos, L. Anton, R. A. Bell, A. Bhandari, G. A. Bramley, R. J. Charlton, R. J. Clements, D. J. Cole, G. Constantinescu, F. Corsetti, S. M.-M. Dubois, K. K. B. Duff, J. M. Escartín, A. Greco, Q. Hill, L. P. Lee, E. Linscott, D. D. O'Regan, M. J. S. Phipps, L. E. Ratcliff, Á. Ruiz Serrano, E. W. Tait, G. Teobaldi, V. Vitale, N. Yeung, T. J. Zuehlsdorff, J. Dziedzic, P. D. Haynes, N. D. M. Hine, A. A. Mostofi, M. C. Payne and C.-K. Skylaris, The ONETEP linear-scaling density functional theory program, *J. Chem. Phys.*, 2020, **152**, 174111, DOI: 10.1063/5.0004445.

26 C.-K. Skylaris, A. A. Mostofi, P. D. Haynes, O. Diéguez and M. C. Payne, Nonorthogonal generalized Wannier function pseudopotential plane-wave method, *Phys. Rev. B: Condens. Matter Mater. Phys.*, 2002, **66**, 035119, DOI: 10.1103/PhysRevB.66.035119.

27 J. P. Perdew, K. Burke and M. Ernzerhof, Generalized Gradient Approximation Made Simple, *Phys. Rev. Lett.*, 1996, **77**, 3865, DOI: 10.1103/PhysRevLett.77.3865.

28 S. Grimme, Semiempirical GGA-type density functional constructed with a long-range dispersion correction, *J. Comput. Chem.*, 2006, **27**, 1787–1799, DOI: 10.1002/jcc.20495.

29 Á. Ruiz-Serrano and C.-K. Skylaris, A variational method for density functional theory calculations on metallic systems with thousands of atoms, *J. Chem. Phys.*, 2013, **139**, 054107, DOI: 10.1063/1.4817001.

30 A. H. Larsen, J. J. Mortensen, J. Blomqvist, I. E. Castelli, R. Christensen, M. Dułak, J. Friis, M. N. Groves, B. Hammer, C. Hargus, E. D. Hermes, P. C. Jennings, P. B. Jensen, J. Kermode, J. R. Kitchin, E. L. Kolsbjerg, J. Kubal, K. Kaasbjerg, S. Lysgaard, J. B. Maronsson, T. Maxson, T. Olsen, L. Pastewka, A. Peterson, C. Rostgaard, J. Schiøtz, O. Schütt, M. Strange, K. S. Thygesen, T. Vegge, L. Vilhelmsen, M. Walter, Z. Zeng and K. W. Jacobsen, The Atomic Simulation Environment-A Python Library for Working with Atoms, *J. Phys.: Condens. Matter*, 2017, **29**, 273002, DOI: 10.1088/1361-648X/aa680e.

31 *CrystalMaker®: a crystal and molecular structures program for Mac and Windows, 9.0.3*, CrystalMaker Software Ltd, Oxford, England, 2014, https://www.crystalmaker.com.

32 A. Kordatos, K. Mohammed, R. Vakili, A. Goguet, H. Manyar, E. Gibson, M. Carravetta, P. Wells and C.-K. Skylaris, Atomistic simulations on the carbidisation processes in Pd nanoparticles, *RSC Adv.*, 2023, **13**, 5619–5626, DOI: 10.1039/D2RA07462A.

33 M. Crespo-Quesada, S. Yoon, M. Jin, A. Prestianni, R. Cortese, F. Cárdenas-Lizana, D. Duca, A. Weidenkaff and L. Kiwi-Minsker, Shape-Dependence of Pd Nanocrystal Carburization during Acetylene Hydrogenation, *J. Phys. Chem. C*, 2015, **119**, 1101, DOI: 10.1021/jp510347r.